JACS
JOURNAL OF THE AMERICAN CHEMICAL SOCIETY
Article
Cite This: J. Am. Chem. Soc. 2017, 139, 14668-14675
pubs.acs.org/JACS

Controlling Dipole Orientation through Curvature: Aromatic Foldamer Bent β-Sheets and Helix−Sheet−Helix Architectures

Arthur Lamouroux,[†,‡] Laure Sebaoun,[†,‡] Barbara Wicher,[†,⊥] Brice Kauffmann,[§] Yann Ferrand,[†] Victor Maurizot,[†] and Ivan Huc*[,†,∥]

[†]Université de Bordeaux, CNRS, Bordeaux Institut National Polytechnique, CBMN (UMR 5248), Institut Européen de Chimie Biologie, 2 Rue Escarpit, 33600 Pessac, France

[§]Université de Bordeaux, CNRS, INSERM, Institut Européen de Chimie Biologie (UMS3033/US001), 2 Rue Escarpit, 33600 Pessac, France

Supporting Information

ABSTRACT: The helix, turn, and β-strand motifs of biopolymer folded structures have been found to prevail also in non-natural backbones. In contrast, foldamers with aryl rings in their main chains possess distinct conformations that may give access to folded objects beyond the reach of peptidic and nucleotidic backbones. In search of such original architectures, we have explored the effect of bending aromatic amide β-sheets using building blocks that impart curvature. Cyclic and multiturn noncyclic sequences were synthesized, and their structures were characterized in solution and in the solid state. Stable bent-sheet conformations were shown to prevail in chlorinated solvents. In these structures, folding overcomes intramolecular electrostatic repulsions and forces local dipoles in each layer of the stacked strands to align in a parallel fashion. Sequences having helical segments flanking a central bent aromatic β-sheet were then synthesized and shown to form well-defined helix−turn−helix architectures in which helical and sheet subcomponents conserve their respective integrity. These objects have a unique basket shape; they possess a cavity the depth and width of which reflects the curvature of the β-sheet segment. They can be compared to previously described helical closed-shell receptors in which a window has been open, thus providing a means to control guest binding and release pathways and kinetics. As a proof of concept, guest binding to one of the helix−sheet−helix structures is indeed found to be fast on the NMR time scale while it is generally slow in the case of helical capsules.

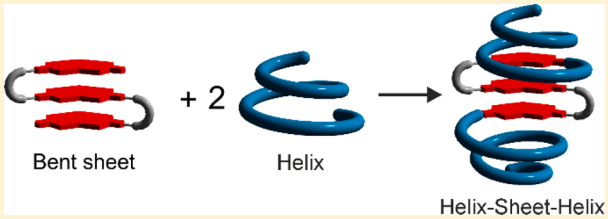

INTRODUCTION

The structures of biopolymers demonstrate the efficiency of folding as an approach to construct atomically precise arrays of chemical groups in space. Folding may counterbalance local repulsions and enforce the proximity of desired functionalities even in disfavored relative orientations. As exemplified by the catalytic properties of enzymes' active sites, unique functions may arise from folding-based conformational control. In the last two decades, this knowledge has been the source of inspiration for chemists to design a wide range of artificial folded architectures termed foldamers.[1] Chemically diverse foldamer backbones have been reported, but, quite remarkably, their structures were found to be less diverse, with an overwhelming prevalence of the helix, turn, and linear-strand secondary motifs common in biopolymers. In this context, foldamers that have aromatic groups in their main chain bear special interest in that they may give access to unusual folded patterns, some of which are beyond the reach of biopolymers. Prominent examples include pillars,[2] knots and interlocked macrocycles,[3] spiral-like objects,[4] and herringbone helices.[5] A remarkable architecture is that of a helix whose diameter may increase and decrease along the sequence (Figure 1E), thus creating a cavity within a secondary folded motif in which outstanding molecular-recognition properties have been evidenced.[6] Just like peptidic and nucleotidic structures and functions differ because the backbones of peptides and nucleotides are chemically distinct, it may be envisaged that the chemically distinct backbones of aromatic foldamers give access to structures and functions different from those of peptides and nucleotides.

In the context of our investigations on aromatic oligoamide foldamers, we have characterized multistranded aromatic β-sheets.[7,8] Examples of artificial sheets in the foldamer literature are rare in comparison to helices. Unlike helices that fulfill their potential for noncovalent interactions intramolecularly, sheets may also engage in intermolecular interactions and form large aggregates that are prone to precipitation, e.g., amyloid fibrils, and thus complicate structural investigations. Hence, β-sheet models based on hydrogen bonds are often designed to be monomeric[9] or dimeric.[10] Our aromatic multiturn β-sheets involved a balanced set of noncovalent interactions strong enough to operate intramolecularly to promote folding and yet weak enough to prevent aggregation. This first generation of aromatic β-sheets was composed of stacks of linear aryl−amide segments connected by dinitrophenyl turns (Figure 1A). The nitro groups hydrogen bond to neighbor aryl−amines, while

Received: July 28, 2017
Published: October 2, 2017

DOI: 10.1021/jacs.7b07961
J. Am. Chem. Soc. 2017, 139, 14668−14675

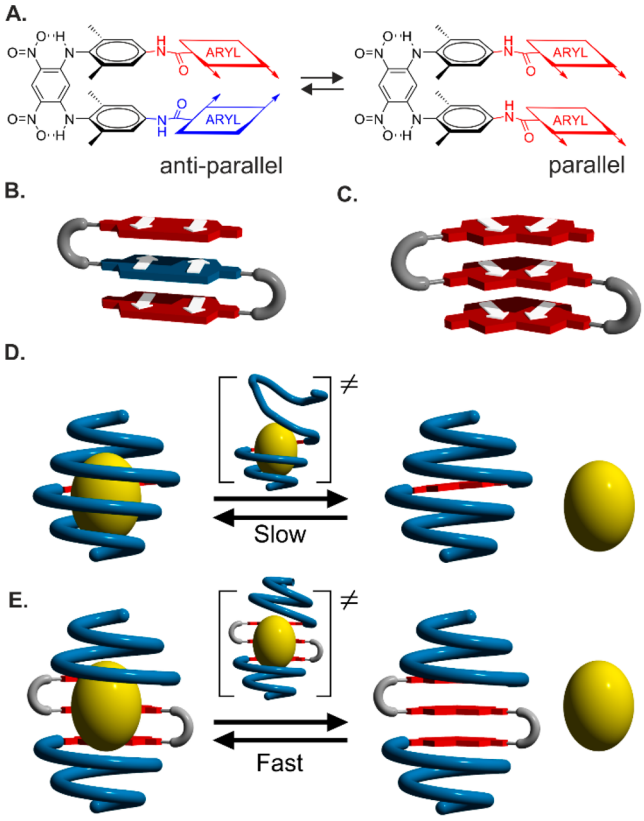

Figure 1. (A) Structure of aromatic β-sheet turn units and equilibrium between antiparallel and parallel arrangements. (B) Antiparallel arrangements of strands in linear aromatic sheets. (C) Parallel arrangements of strands in bent aromatic sheets. (D) Schematic representation of a C_2 symmetrical helical capsule that must unfold to bind and release a guest. (E) Schematic representation of a helix−sheet−helix architecture that can bind and release a guest with minimal perturbation of its structure. Aromatic strands are represented as rectangular objects, whereas turns and helix segments are shown as gray and blue tubes, respectively. White arrows in B and C schematize the orientation of local dipoles.

the methyl groups of two adjacent xylyl rings set their orientation parallel to each other in planes roughly perpendicular to the plane of the dinitrophenyl ring. Aryl moieties attached to the xylyl rings then stack in a face-to-face arrangement that, in principle, may be antiparallel or parallel (Figure 1A). We found that antiparallel organization was favored (Figure 1B) as, for example, in macrocycle **1** (Chart 1). This preference results from the effect of local dipoles and is generally observed upon stacking polar aromatic rings in the solid state or in aggregates.[11]

In the following, we present a study of the effect of bending on the conformation of these aromatic β-sheets. We find that introducing curvature effectively enforces the formation of stacks of aryl rings in which local dipoles are parallel despite the repulsions associated with this arrangement (Figure 1C). In such bent structures, an antiparallel orientation would give rise to misfolding with reduced $\pi-\pi$ overlap. Parallel orientations are favored as they maximize $\pi-\pi$ overlap. This relationship between bending and polarity, a notion common in the field of liquid crystals,[12] is significant because parallel dipole arrangements are a much-sought-after property in materials, for example, in the context of their nonlinear optical responses.[13] Furthermore, we demonstrate that bent aromatic β-sheets can

Chart 1. Linear (1) or Bent (2−4) Macrocyclic and Multiturn Aromatic Oligoamide β-sheets

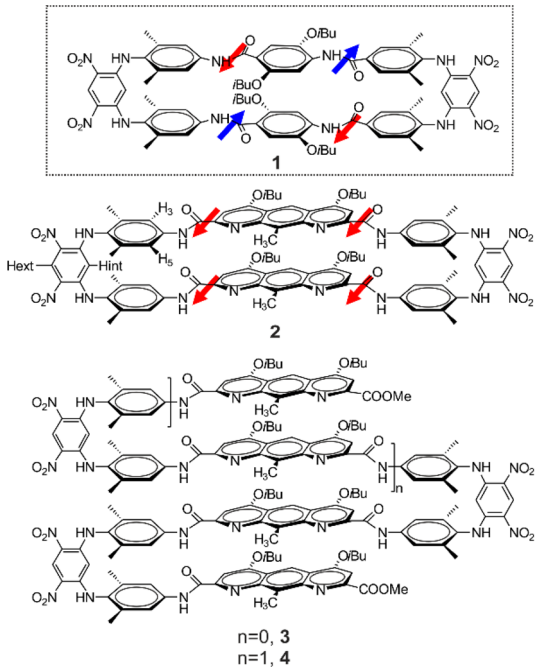

be combined with aromatic helices. Aromatic helix−sheet−helix folded structures were generated that, to the best of our knowledge, constitute the first examples of aromatic foldamers composed of more than one kind of secondary motif and, significantly, possess an unprecedented architecture. Indeed, the introduction of aromatic β-sheets within the wall of a helical capsule (part D vs E of Figure 1) amounts to creating a basket-like object having a window of defined size and provides a means to fine-tune guest binding and release pathways and kinetics to and from the basket cavity. We bring proof of concept of this design feature by showing that an α-hydroxy acid guest exchanges rapidly on the NMR time scale from these open receptors whereas exchange was found to be slow in closed-shell helical receptors. Thus, the helix−turn−helix structures further demonstrate the ability of aromatic backbones to adopt shapes beyond the reach of peptides, nucleotides, and related backbones.

RESULTS AND DISCUSSION

Bent β-sheet Architectures. The induction of curvature within aromatic β-sheets was made possible by connecting dinitro−di(xylylamino)−phenyl turns using aromatics with substituents at an angle different from 180°. For this purpose, we used pyrido[3,2-*g*]quinolinedicarboxylic acids, which we refer to as 1,8-diaza-2,7-anthracenedicarboxylic acids.[11d,14] Prior to preparing multistranded turns, we tested the validity of our design in a one-step macrocyclization reaction. A diaza-anthracene diacid was coupled to a diamine-functionalized turn using PyBOP (benzotriazol-1-yl-oxytripyrrolidinophosphonium hexafluorophosphate) as an activating agent to produce macrocycle **2** in an unoptimized 24% yield.

A crystal structure of **2** demonstrated the expected parallel arrangement of the stacked diaza-anthracenes (Figure 2A and B). The top view shows that aryl rings are slightly offset but that local dipoles are strictly parallel. An energy-minimized model of the antiparallel noncyclic amino acid precursor of **2**

DOI: 10.1021/jacs.7b07961
J. Am. Chem. Soc. 2017, 139, 14668−14675

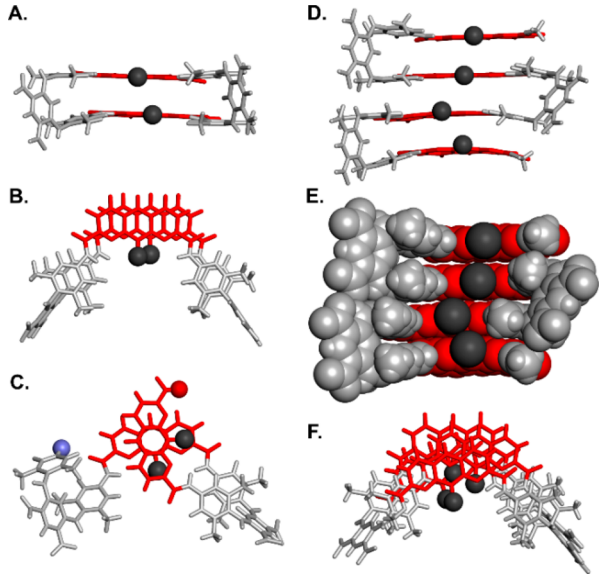

Figure 2. (A) Side view and (B) top view of the crystal structure of macrocycle **2**; (C) top view of the energy-minimized model conformation (Maestro version 6.5 using the MMFFs force field) of macrocycle **2** precursor as an antiparallel conformer. (D, E) Side views and (F) top view of the crystal structure of tridecamer **4**. In (D) and (F) **4** is shown in tube representation, whereas it appears in CPK representation in (E). In all the representations the turns are shown in light gray whereas the bent diaza-anthracenes appear in red. Methyl groups of diaza-anthracenes are shown as black spheres. In (C), acid and amine terminal groups are shown as red and blue spheres, respectively. Isobutoxy side chains have been omitted for clarity.

illustrates the reduced aromatic $\pi-\pi$ overlap and a large distance between amine and acid functions that presumably precludes cyclization in this conformation (Figure 2C). In solution, the sharp ^{1}H NMR spectrum of **2** (Figure 3A) was fully assigned using multidimensional experiments[15] (see Supporting Information). H_{int} protons as defined in Chart 1 are shielded down to 4.76 ppm, reflecting strong ring-current effects by the xylyl rings above and below. CH_2 protons of isobutoxy chains, H_3 and H_5 protons of xylyl groups (at 8.38 and 6.69 ppm), and even the protons of the two xylyl CH_3 groups are all anisochronous, indicating slow dynamics of the structure. The anisochronicity of the xylyl CH_3 protons, despite a small chemical shift difference ($\Delta\delta$ = 0.02 ppm at 300 MHz), implies that exchange by rotation of the xylyl units is slower than 7.71 Hz. No exchange could be observed in rotating frame nuclear Overhauser effect spectroscopy (ROESY) spectra. Furthermore, no change of the spectrum was observed from −50 °C (in $CDCl_3$) to +80 °C (in $C_2D_2Cl_4$, Figure S1). These results overall support the formation of a single conformer with remarkably slow dynamics. By comparison, slow exchange between the H_3 and H_5 xylyl protons of macrocycle **1** was only observed upon cooling.[7]

We then proceeded with the synthesis of tristranded sheet **3** and tetrastranded sheet **4** (Scheme S2). A key step was the desymmetrization of the diamine-functionalized turn using 1 equivalent of a diaza-anthracene monoacid monoester. A crystal structure of **4** (Figure 2D−F) confirmed the features revealed by the bent-sheet structure of macrocycle **2**. The noncyclic nature of **4** offers additional conformational degrees of freedom, and offsetting between aryl rings and tilting of turn units away from 90° are more pronounced than in the structure of **1**.

Nevertheless, the structure does consist of a stack of four diaza-anthracene rings with all their local dipoles parallel.

In solution the NMR spectra of **3** and **4** were both fully assigned using multidimensional experiments[15] (see Supporting Information). The results corroborated the solid-state structure of **4**. Evidence for folding in multistranded bent-sheet conformations came for nuclear Overhauser effect (NOE) correlations between the different 9-methylanthracene protons, both in **3** and **4** (Figure S4): proximity between these methyl groups is only allowed in the parallel arrangement of the diaza-anthracene units. NMR also indicates faster dynamics in the noncyclic structures than in **2** and that sheet stability increases upon increasing strand length, suggesting a certain degree of cooperativity. For instance, H_3 and H_5 protons of each xylyl group of **3** exchange rapidly on the NMR time scale at 50 °C and the signals are coalesced at 10 °C (Figure S2), whereas slow exchange is observed for **4** at 10 °C (Figure 3C). The spectra of **4** (but not the spectra of **3**) display anisochronicity of the CH_2 protons of isobutoxy chains and of the protons of the xylyl CH_3 groups. Nevertheless, dynamics in **4** are faster than in macrocycle **2**: exchange is fast on the NMR time scale at 80 °C

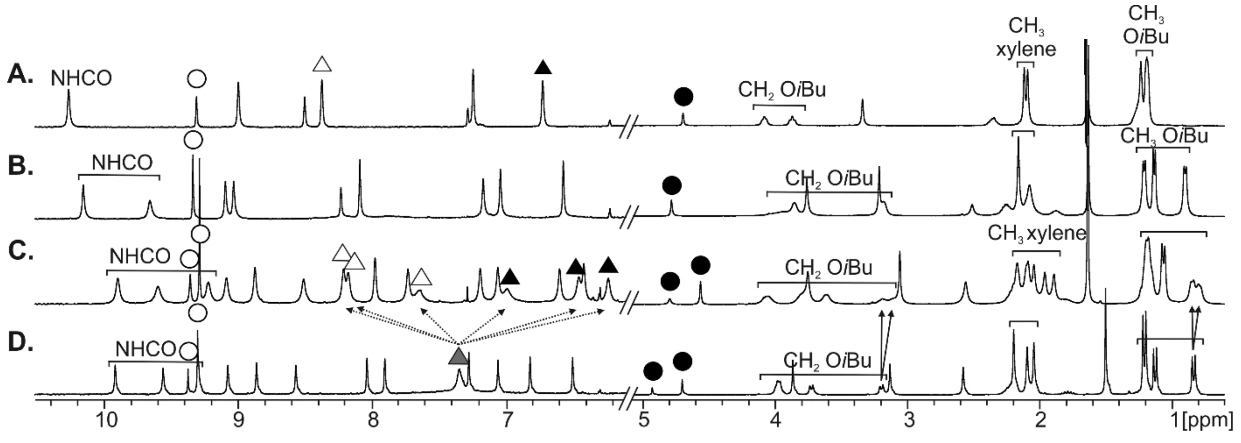

Figure 3. Part of the 300 MHz ^{1}H NMR spectra in $C_2D_2Cl_4$ at 10 °C of (A) macrocycle **2**; (B) nonamer **3**; (C) tridecamer **4**; and (D) tridecamer **4** at 80 °C. Signals of H_{ext} are marked with white circles. Signals of H_{int} are marked with black circles. H_3 and H_5 signals of xylene units are marked with white and black triangles, respectively. H_3 + H_5 fast exchange average signal is marked by a gray triangle. Diastereotopic protons belonging to isobutoxy side chains are marked by solid arrows.

DOI: 10.1021/jacs.7b07961
J. Am. Chem. Soc. 2017, 139, 14668−14675

(Figure 3D) and correlations can be observed in ROESY maps in the slow-exchange regime at lower temperatures.

Helix−Sheet−Helix Architectures. The well-behaved folding of aromatic bent β-sheets was further explored in combination with helically folded segments within longer sequences. We surmised that an aromatic helix connected at the end of a bent sheet would simply stack on top of it without any detrimental interference, and we decided to test this prediction using helical segments, the diameter of which varies along the sequence. These variable-diameter segments are key components of aromatic foldamer-based helical capsules that recognize guest molecules in their cavity with high selectivity and affinity.[6b,c] A capsule shape with its characteristic reduced diameter at both ends is schematized in Figure 1D. An interesting aspect of these molecular containers is that they completely isolate their guest from the solvent. For a guest to come in and out, the helix has to partially unfold, a given unit generally playing the role of a hinge to temporarily open a passage.[16] As a consequence, binding and release kinetics are all the more slow when the guest is large, e.g., slow exchange on the NMR time scale is reached below −55 °C for a water molecule guest[17] and persists above 50 °C for a monosaccharide.[6b] The introduction of a bent sheet between two variable-diameter helix segments thus amounts to permanently opening a sort of window in a capsule wall. As shown below, the size of the window may be tuned according to the curvature imparted by the bent aromatic β-sheet. This provides a means to enhance and fine-tune guest and binding release kinetics.

Foldamers **5**−**8** (Chart 2) were prepared as described in the Supporting Information. They all contain one (**8**) or two (**5**−**7**) helical oligoamide segments composed of two 7-amino-1,8-naphthyridine-2-carboxylic acid, one 2,6-diamino-pyridine, and three 8-amino-2-quinolinecarboxylic acid at the more curved end, as well as one (**8**) or two (**5**−**7**) turn units. The connections between the turn units vary. In **5**, the connecting element is itself a 1,8-diaza-2,7-anthracenedicarboxylic acid. The central sheet of **5** is thus identical to compound **3**. In **6**, the central pyridine−pyridazine−pyridine motif is slightly longer than a diaza-anthracene, but it imparts a higher curvature because the angle between the two carboxylic acid functions is reduced.[16a,18] The urea function of **7** is a very short linkage imparting low curvature—two distinct conformers may be expected depending on whether the urea aligns itself one way or the other with respect to the anthracenes above and below.

Crystal structures of **6a** and **7** as well as an energy-minimized molecular model of **5** confirmed the formation of the anticipated folding (Figure 4A−O). In all structures, a central sheet segment is flanked by two helices, giving rise to basket-like objects, the openings of which depend on the degree of curvature of the sheet. Thus, the structure of **6a** has a deeper and narrower cavity, while the structure of **7** possesses the widest opening, with the structure of **5** showing an intermediate situation. In the structure of **7**, the urea carbonyl oxygen points toward the cavity. It is worth noting that, regardless of the sheet curvature, the overhanging helical segments do not collapse in the cavity and that all folded secondary motifs retain their integrity in these structures. A somewhat unexpected result came from the structure of **8**, which revealed a dimerization process in which the peripheral strands of two sheets interdigitate (Figure 4P−T). The outcome is a basket that much resembles the structures of **5**−**7**, even though **8** itself is only about half the size of **5**. Because they all comprise a two-turn β-sheet, all structures also possess an average C_2 symmetry

Chart 2. Formula of Helix−Sheet−Helix Oligomers

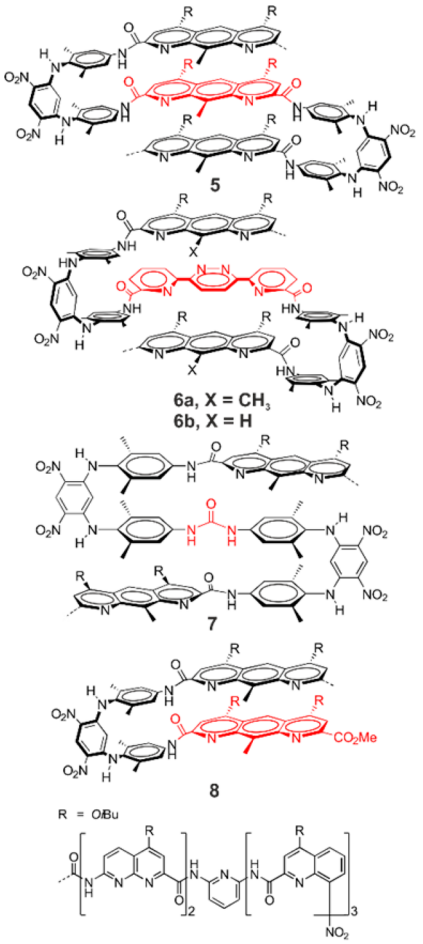

axis perpendicular to the axis of the helix segments. Consequently, the two helices of a given sequence possess the same handedness. However, one can predict that sheets with an odd number of turns would be flanked with helices having opposite handedness, the sheet triggering handedness inversion[19] and the overall structure being plane symmetrical.

In solution, sharp and well-resolved NMR spectra suggest that **5**−**8** adopt well-defined conformations (Figure 5). Amide and aromatic resonances are spread over a wide chemical shift range, reflecting the combined effects of hydrogen bonding involving amide protons, which cause downfield shifts of their resonances, and ring-current effects associated with aromatic stacking, which cause upfield shifts. The methyl groups of the xylyl units are under rapid exchange at room temperature, indicating fast conformational dynamics. Yet their resonances are found below 2 ppm, i.e., at lower chemical shift values than in macrocycle **2** (Figure 3A), as a consequence of the stacking of the helical segments. Similarly, H_{int} protons in **5**−**8** are even more shielded (signals below 4.5 ppm) than in β-sheets **2**−**4** (Figure 3 and Figure S5).

Solution studies of **8** were carried out in $CDCl_3$ and supported the existence in solution of the dimer observed in the solid state (Figure 4P−T). Upon increasing concentration, a new set of resonances appeared assigned to the formation of duplex $(\mathbf{8})_2$ (in red, Figure 6A−E). Diffusion-ordered spectroscopy (DOSY) experiments (Figure S7) allowed for the calculation of the diffusion coefficients of the monomer (4.84^{-10} m^2/s) and of the dimer (4.73^{-10} m^2/s). The

DOI: 10.1021/jacs.7b07961
J. Am. Chem. Soc. 2017, 139, 14668−14675

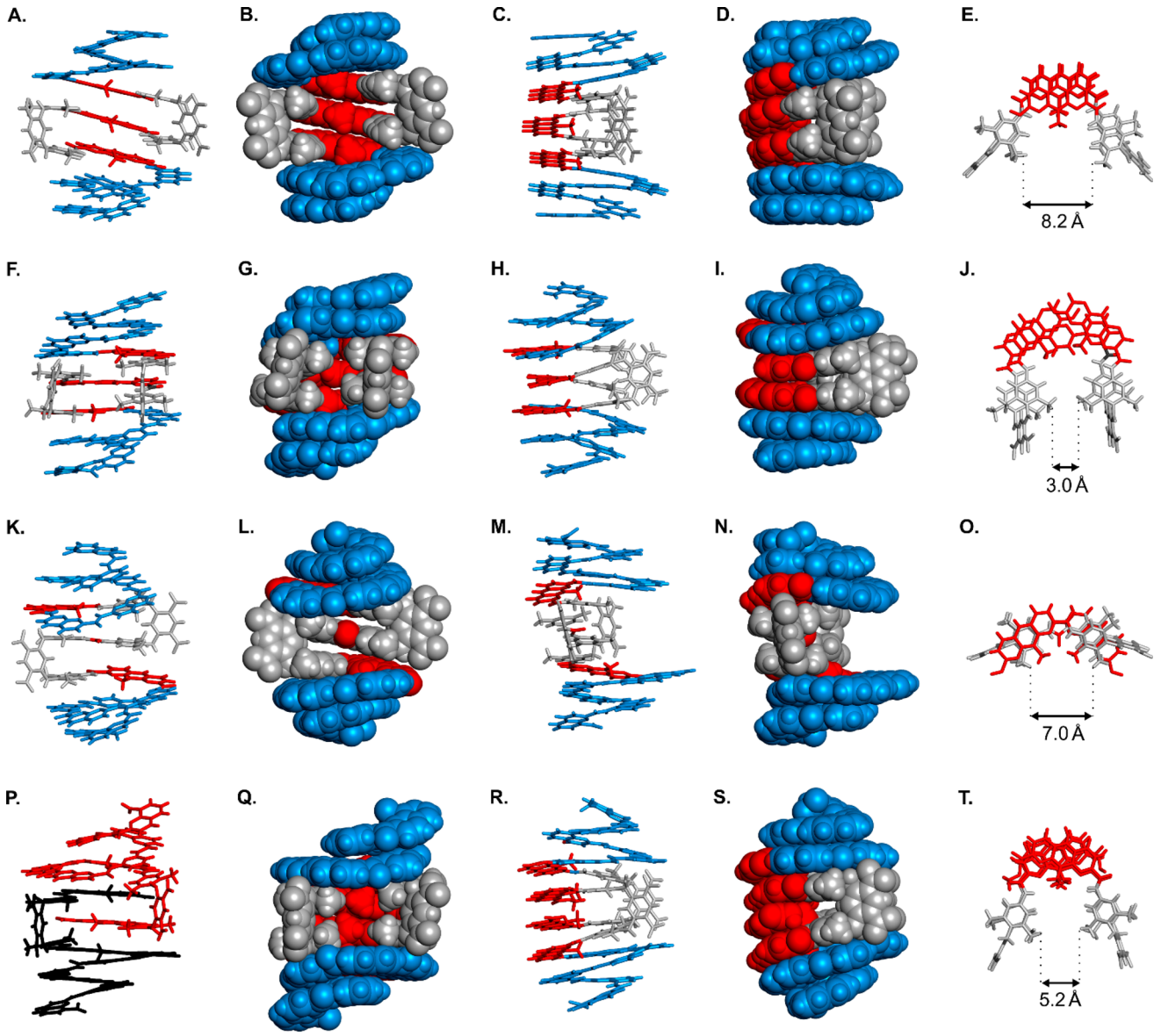

Figure 4. (A–E) Energy-minimized molecular model using the Merck molecular force field static (MMFFs) of oligomer **5**. Structures in the solid state analyzed by single-crystal X-ray crystallography of (F–J) oligomer **6a**; (K–O) oligomer **7**; and (P–T) duplex $(\mathbf{8})_2$. In all representations except (P), the helical cones are shown in blue, the diaza-anthracene units are shown in red, and the turn units are shown in white. In (K) the intercalated strands of the duplex $(\mathbf{8})_2$ are highlighted in red and black. (E), (J), (O), and (T) show a top view of the helix–sheet–helix architectures in which both helical cones have been omitted. This view highlights the varying orientations of the turn units. In (A–T) isobutoxy side chains and included solvent molecules were omitted for clarity. Only the all-P helical isomers are shown. The structures belong to centrosymmetrical space groups and thus also contain the all-M isomers.

monomeric and dimeric forms are in slow exchange on the NMR time scale (Figure 6) despite the limited overlap associated with the reciprocal intercalation observed in the solid state. Integration of the signals allows for the calculation of the dimerization constant K_{dim} = 47 L·mol^{-1} in $CDCl_3$. The amide protons of the duplex are shielded compared to the monomeric form that prevails at lower concentration.

Another dynamic parameter concerns the orientation of the urea function of **7**. In the solid-state structure, the urea carbonyl group was found to point toward the cavity of the molecule, whereas the NH pointed toward the solvent. Modeling studies show that changes of this orientation may result in different curvatures of the molecule (Figures S15 and S16). Although it was not possible to assign the NMR spectrum of **7** (Figure 5) to one or another conformer, its sharpness suggests that one conformation prevails or that different conformers exchange fast despite significant structural rearrangements.

Sequences **5**–**8** were not designed to bind to any particular guest. Nevertheless, their quinoline–pyridine–naphthyridine helical segments have been shown before to hydrogen bond to α-hydroxy acids, and capsules containing these segments may bind to tartaric or malic acid.[6c,16,18] Titrations were thus carried out using glycolic acid as a guest. However, no clear binding was detected in the case of **5**, **6a**, and **7**. This was attributed to the 9-methyl groups of the 1,8-diaza-anthracene units that protrude at the entrance of the site where hydroxy acids are expected to bind. Sequence **6b**, which lacks these methyl groups, was thus synthesized (Chart 2). Titration with glycolic acid in $CDCl_3/D_6$-acetone (9:1 vol/vol) at 25 °C resulted in chemical shift variations consistent with rapid binding and

DOI: 10.1021/jacs.7b07961
J. Am. Chem. Soc. 2017, 139, 14668–14675

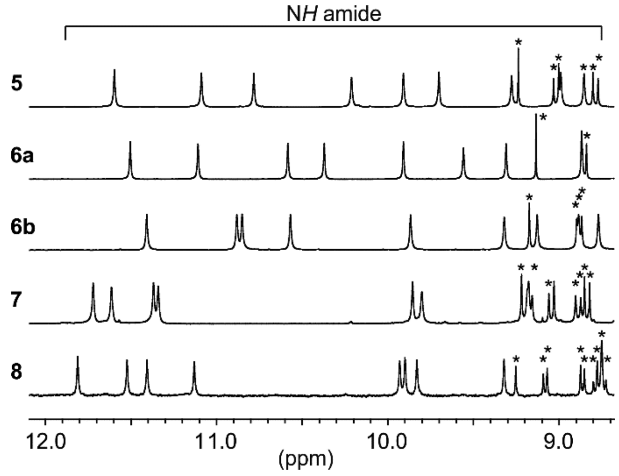

Figure 5. Excerpts of ^{1}H NMR spectra (400 MHz, 25 °C) showing the amide resonances in $CDCl_3$ of **5** (1 mM), **6a** (1 mM), **6b** (1 mM), **7** (1 mM), and the monomeric form of oligomer **8** (0.5 mM). Stars denote aromatic resonances.

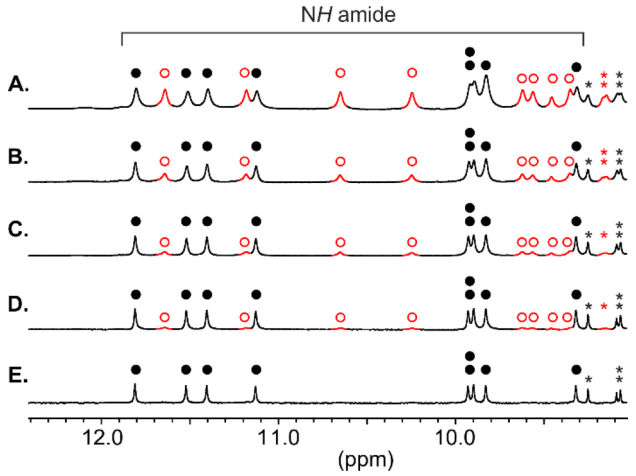

Figure 6. Excerpts of the 400 MHz ^{1}H NMR spectra in $CDCl_3$ at 25 °C of **8** at (A) 10 mM; (B) 5 mM; (C) 2 mM; (D) 1 mM; and (E) 0.5 mM. Signals of the amide protons belonging to single-stranded **8** are marked with full black circles, and those belonging to the duplex $(\mathbf{8})_2$ are marked with empty red circles.

release on the NMR time scale (Figure 7). Using HypNmr (2008, version 4.0.71),[20] chemical shift values could be fitted well to a 1:2 binding isotherm, consistent with the two binding sites of **6b**. The first and second association constants, K_1 = 121 L·mol^{-1} and K_2 = 162 L·mol^{-1}, albeit not very strong, revealed a certain degree of positive cooperative (α = 5).[21]

Rapid guest exchange on the NMR time scale contrasts with the slow guest exchange observed in closed-shell helical containers of the kind shown in Figure 1D.[6b,c,16] This suggests that the guest is bound through the open side of the basket-like host and therefore that both the binding pathway and the binding kinetics may be modulated through the design of the basket structural features.

CONCLUSION

Aromatic amide β-sheets may adopt stable bent conformations upon introducing building blocks that impart curvature. In these structures, folding overcomes intramolecular electrostatic repulsions and forces local dipoles in each layer of the stacked

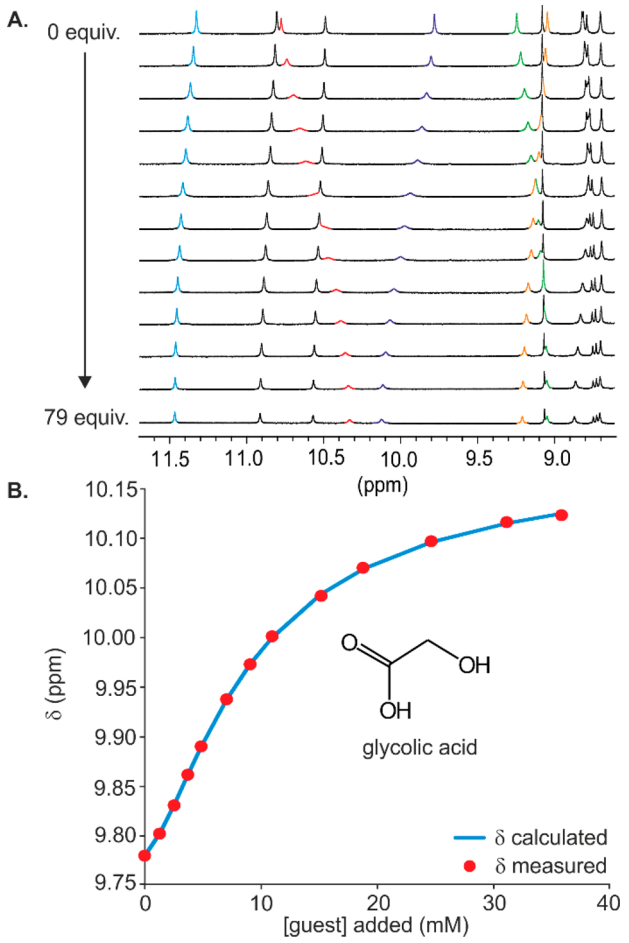

Figure 7. (A) ^{1}H NMR titration experiment (400 MHz, 25 °C) in $CDCl_3/D_6$-acetone (9:1, vol/vol) of **6b** (1 mM) in the presence of 0, 1.3, 2.6, 3.9, 5.3, 7.9, 10.5, 13.1, 19.7, 26.3, 39.4, 59.2, and 78.9 equiv of glycolic acid. (B) Experimental and calculated values using a 1:2 binding model for the NMR binding study of oligomer **6b** vs glycolic acid in $CDCl_3/D_6$-acetone (9:1, vol/vol). Resonance at 9.78 ppm was used for the analysis.

strands to align in a parallel fashion. Furthermore, sequences having helical segments flanking a central bent aromatic β-sheet were shown to form well-defined helix−turn−helix architectures in which helical and sheet subcomponents conserve their respective integrity. Our results thus provide new examples of how foldamers with aryl rings in their main chain may give access to original and engineerable folded structures that would be difficult to produce from peptides, nucleotides, and related foldamer backbones. The possibility to tailor an opening of predictable size within the wall of a helically folded receptor represents a step toward controlling guest binding and release pathways and kinetics (Figure 1D and E), a prospect of interest considering recent achievements using aromatic foldamers in the field of molecular recognition.[6,16] Helix−turn−helix motifs may also help access topologically complex objects through the winding of open-ended helices around dumbbell guests to form so-called foldaxanes. Foldaxanes have already been produced using rodlike guests and single-helical or double-helical hosts (Figure 8A).[22] When the host is a helix−turn−helix, foldaxane formation may proceed through original pathways and be compatible with T-shaped or X-shaped guests (Figure 8B and C). Finally, foldamer structures composed of several and distinct secondary subcomponents represent an important and

DOI: 10.1021/jacs.7b07961
J. Am. Chem. Soc. 2017, 139, 14668−14675

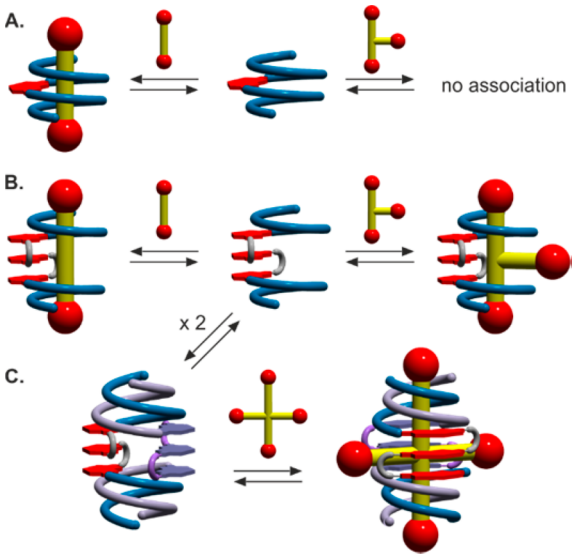

Figure 8. Host–guest topologies that can be expected from the association of dumbbell guests and an open-ended helix[22] (A), a helix–turn–helix (B), or a duplex formed from two helix–turn–helix structures (C).

challenging objective toward the implementation of sophisticated function.[10e,f,23] The helix–sheet–helix architectures described here constitute an original development in this respect and complement objects produced from helices only.[23]

■ ASSOCIATED CONTENT

Supporting Information

The Supporting Information is available free of charge on the ACS Publications website at DOI: 10.1021/jacs.7b07961.

Experimental details for synthetic procedures, spectroscopic data, and molecular modeling (PDF)
Crystallographic information file for **2** (CIF)
Crystallographic information file for **4** (CIF)
Crystallographic information file for **6** (CIF)
Crystallographic information file for **7** (CIF)
Crystallographic information file for **8** (CIF)

■ AUTHOR INFORMATION

Corresponding Author

*ivan.huc@cup.lmu.de

ORCID

Barbara Wicher: 0000-0003-2254-2508
Brice Kauffmann: 0000-0002-2932-3255
Yann Ferrand: 0000-0002-6552-6914
Ivan Huc: 0000-0001-7036-9696

Present Addresses

[⊥]B.W.: Department of Chemical Technology of Drugs, Poznan University of Medical Sciences, Grunwaldzka 6, 60-780 Poznan, Poland.
[∥]I.H.: Department of Pharmacy, Ludwig-Maximilians-Universität, Butenandtstr. 5, 81377 München, Germany.

Author Contributions

[‡]A.L. and L.S. contributed equally to this work.

Notes

The authors declare no competing financial interest.

■ ACKNOWLEDGMENTS

This work was supported by the European Research Council under the European Union's Seventh Framework Programme (Grant agreement no. ERC-2012-AdG-320892). We thank Dr. G. Lautrette for providing advanced synthetic precursor **19**. We gratefully acknowledge the ESRF for beam time on ID29 and Christoph Muller-Dieckmann for technical assistance. This work has benefited from the facilities and expertise of the Biophysical and Structural Chemistry platform at IECB, CNRS UMS3033, INSERM US001, Bordeaux University, France.

■ REFERENCES

(1) (a) Guichard, G.; Huc, I. *Chem. Commun.* **2011**, *47*, 5933–5941. (b) Gellman, S. H. *Acc. Chem. Res.* **1998**, *31*, 173–180. (c) Hill, D. J.; Mio, M. J.; Prince, R. B.; Hughes, T. S.; Moore, J. S. *Chem. Rev.* **2001**, *101*, 3893–4011.
(2) (a) Lokey, R. S.; Iverson, B. L. *Nature* **1995**, *375*, 303–305. (b) Ghosh, S.; Ramakrishnan, S. *Angew. Chem., Int. Ed.* **2004**, *43*, 3264–3268.
(3) (a) Brüggemann, J.; Bitter, S.; Müller, S.; Müller, W. M.; Müller, U.; Maier, N. M.; Lindner, W.; Vögtle, F. *Angew. Chem., Int. Ed.* **2007**, *46*, 254–259. (b) Ponnuswamy, N.; Cougnon, F. B. L.; Clough, J. M.; Pantoş, G. D.; Sanders, J. K. M. *Science* **2012**, *338*, 783–785. (c) Chung, M.-K.; White, P. S.; Lee, S. J.; Gagné, M. R. *Angew. Chem., Int. Ed.* **2009**, *48*, 8683–8686. (d) Chung, M.-K.; White, P. S.; Lee, S. J.; Waters, M. L.; Gagné, M. R. *J. Am. Chem. Soc.* **2012**, *134*, 11415–11429. (e) Chung, M.-K.; Lee, S. J.; Waters, M. L.; Gagné, M. R. *J. Am. Chem. Soc.* **2012**, *134*, 11430–11443. (f) Chung, M.-K.; White, P. S.; Lee, S. J.; Gagné, M. R.; Waters, M. L. *J. Am. Chem. Soc.* **2016**, *138*, 13344–13352.
(4) Hunter, C. A.; Spitaleri, A.; Tomas, S. *Chem. Commun.* **2005**, 3691–3693.
(5) (a) Delsuc, N.; Godde, F.; Kauffmann, B.; Léger, J.-M.; Huc, I. *J. Am. Chem. Soc.* **2007**, *129*, 11348–11349. (b) Kudo, M.; Carbajo López, D.; Maurizot, V.; Masu, H.; Tanatani, A.; Huc, I. *Eur. J. Org. Chem.* **2016**, *2016*, 2457–2466. (c) Akazome, M.; Ishii, Y.; Nireki, T.; Ogura, K. *Tetrahedron Lett.* **2008**, *49*, 4430–4433.
(6) (a) Hua, Y.; Liu, Y.; Chen, C.-H.; Flood, A. H. *J. Am. Chem. Soc.* **2013**, *135*, 14401–14412. (b) Chandramouli, N.; Ferrand, Y.; Lautrette, G.; Kauffmann, B.; Mackereth, C. D.; Laguerre, M.; Dubreuil, D.; Huc, I. *Nat. Chem.* **2015**, *7*, 334–341. (c) Lautrette, G.; Wicher, B.; Kauffmann, B.; Ferrand, Y.; Huc, I. *J. Am. Chem. Soc.* **2016**, *138*, 10314–10322.
(7) (a) Sebaoun, L.; Maurizot, V.; Granier, T.; Kauffmann, B.; Huc, I. *J. Am. Chem. Soc.* **2014**, *136*, 2168–2174. (b) Sebaoun, L.; Kauffmann, B.; Delclos, T.; Maurizot, V.; Huc, I. *Org. Lett.* **2014**, *16*, 2326–2329.
(8) As a relevant background, see also: (a) Lin, L.; Zhang, J.; Wu, X.; Liang, G.; He, L.; Gong, B. *Chem. Commun.* **2010**, *46*, 7361–7363. (b) Prabhakaran, P.; Puranik, V. G.; Chandran, J. N.; Rajamohanan, P. R.; Hofmann, H.-J.; Sanjayan, G. J. *Chem. Commun.* **2009**, 3446–3448. (c) Nair, R. V.; Kheria, S.; Rayavarapu, S.; Kotmale, A. S.; Jagadeesh, B.; Gonnade, R. G.; Puranik, V. G.; Rajamohanan, P. R.; Sanjayan, G. J. *J. Am. Chem. Soc.* **2013**, *135*, 11477–11480. (d) Mrksich, M.; Parks, M. E.; Dervan, P. *J. Am. Chem. Soc.* **1994**, *116*, 7983–7988.
(9) (a) Wyrembak, P. N.; Hamilton, A. D. *J. Am. Chem. Soc.* **2009**, *131*, 4566–4567. (b) German, E. A.; Ross, J. E.; Knipe, P. C.; Don, M. F.; Thompson, S.; Hamilton, A. H. *Angew. Chem., Int. Ed.* **2015**, *54*, 2649–2652. (c) Lingard, H.; Han, J. T.; Thompson, A. L.; Leung, I. K. H.; Scott, R. T. W.; Thompson, S.; Hamilton, A. D. *Angew. Chem., Int. Ed.* **2014**, *53*, 3650–3653.
(10) (a) Nowick, J. S.; Chung, D. M.; Maitra, K.; Maitra, S.; Stigers, K. D.; Sun, Y. *J. Am. Chem. Soc.* **2000**, *122*, 7654–7661. (b) Nowick, J. S.; Brower, J. O. *J. Am. Chem. Soc.* **2003**, *125*, 876–877. (c) Khakshoor, O.; Demeler, B.; Nowick, J. S. *J. Am. Chem. Soc.* **2007**, *129*, 5558–5569. (d) Khakshoor, O.; Lin, A. J.; Korman, T. P.; Sawaya, M. R.; Tsai, S.-C.; Eisenberg, D.; Nowick, J. S. *J. Am. Chem. Soc.* **2010**, *132*, 11622–11628. (e) Cheng, P.-N.; Pham, J. D.; Nowick, J. S. *J. Am.*

DOI: 10.1021/jacs.7b07961
J. Am. Chem. Soc. 2017, 139, 14668–14675

Chem. Soc. **2013**, *135*, 5477−5492. (f) Kreutzer, A. G.; Hamza, I. L.; Spencer, R. K.; Nowick, J. S. *J. Am. Chem. Soc.* **2016**, *138*, 4634−4642. (g) Zhu, J.; Lin, J.-B.; Xu, Y.-X.; Shao, X.-B.; Jiang, X.-K.; Li, Z.-T. *J. Am. Chem. Soc.* **2006**, *128*, 12307−12313. (h) Xu, Y.-X.; Zhan, T.-G.; Zhao, X.; Li, Z.-T. *Org. Chem. Front.* **2014**, *1*, 73−78. (i) Gong, B.; Yan, Y.; Zeng, H.; Skrzypczak-Jankunn, E.; Kim, Y. W.; Zhu, J.; Ickes, H. *J. Am. Chem. Soc.* **1999**, *121*, 5607−5608. (j) Yang, X.; Martinovic, S.; Smith, R. D.; Gong, B. *J. Am. Chem. Soc.* **2003**, *125*, 9932−9933. (k) Gong, B. *Acc. Chem. Res.* **2012**, *45*, 2077−2087. (l) Archer, E. A.; Sochia, A. E.; Krische, M. J. *Chem. - Eur. J.* **2001**, *7*, 2059−2066. (m) Archer, E. A.; Krische, M. J. *J. Am. Chem. Soc.* **2002**, *124*, 5074−5083. (n) Gong, H.; Krische, M. J. *J. Am. Chem. Soc.* **2005**, *127*, 1719−1725.

(11) (a) Yamauchi, Y.; Yoshizawa, M.; Akita, M.; Fujita, M. *J. Am. Chem. Soc.* **2010**, *132*, 960−966. (b) Kishikawa, K.; Furusawa, S.; Yamaki, T.; Kohmoto, S.; Yamamoto, M.; Yamaguchi, K. *J. Am. Chem. Soc.* **2002**, *124*, 1597−1605. (c) Krówczyński, A.; Krzyczkowska, P.; Salamończyk, M.; Górecka, E.; Pociecha, D.; Szydłowska, J. *Liq. Cryst.* **2012**, *39*, 729−737. (d) Berni, E.; Dolain, C.; Kauffmann, B.; Léger, J.-M.; Zhan, C.; Huc, I. *J. Org. Chem.* **2008**, *73*, 2687−2694.

(12) (a) Reddy, R. A.; Tschierske, C. *J. Mater. Chem.* **2006**, *16*, 907−961. (b) Eichhorn, S. H.; Paraskos, A. J.; Kishikawa, K.; Swager, T. M. *J. Am. Chem. Soc.* **2002**, *124*, 12742−12751. (c) Gimeno, N.; Clemente, M. J.; Forcén, P.; Serrano, J. L.; Ros, M. B. *New J. Chem.* **2009**, *33*, 2007−2014.

(13) (a) Datta, A.; Pati, S. K. *Chem. Soc. Rev.* **2006**, *35*, 1305−1323. (b) Datta, A.; Pati, S. K. *J. Chem. Phys.* **2003**, *118*, 8420−8427. (c) Liao, Y.; Firestone, K. A.; Bhattacharjee, S.; Luo, J.; Haller, M.; Hau, S.; Anderson, C. A.; Lao, D.; Eichinger, B. E.; Robinson, B. H.; Reid, P. J.; Jen, A. K.-Y.; Dalton, L. R. *J. Phys. Chem. B* **2006**, *110*, 5434−5438.

(14) Singleton, M. L.; Castellucci, N.; Massip, S.; Kauffmann, B.; Ferrand, Y.; Huc, I. *J. Org. Chem.* **2014**, *79*, 2115−2122.

(15) Dolain, C.; Grélard, A.; Laguerre, M.; Jiang, H.; Maurizot, V.; Huc, I. *Chem. - Eur. J.* **2005**, *11*, 6135−6144.

(16) (a) Ferrand, Y.; Chandramouli, N.; Kendhale, A. M.; Aube, C.; Kauffmann, B.; Grélard, A.; Laguerre, M.; Dubreuil, D.; Huc, I. *J. Am. Chem. Soc.* **2012**, *134*, 11282−11288. (b) Abramyan, A. M.; Liu, Z.; Pophristic, V. *Phys. Chem. Chem. Phys.* **2014**, *16*, 20406−20410.

(17) Garric, J.; Léger, J.-M.; Huc, I. *Angew. Chem., Int. Ed.* **2005**, *44*, 1954−1958.

(18) Ferrand, Y.; Kendhale, A. M.; Kauffmann, B.; Grélard, A.; Marie, C.; Blot, V.; Pipelier, M.; Dubreuil, D.; Huc, I. *J. Am. Chem. Soc.* **2010**, *132*, 7858−7859.

(19) Maurizot, V.; Dolain, C.; Leydet, Y.; Léger, J.-M.; Guionneau, P.; Huc, I. *J. Am. Chem. Soc.* **2004**, *126*, 10049−10052.

(20) (a) Frassineti, C.; Ghelli, S.; Gans, P.; Sabatini, A.; Moruzzi, M. S.; Vacca, A. *Anal. Biochem.* **1995**, *231*, 374−382. (b) Frassineti, C.; Alderighi, L.; Gans, P.; Sabatini, A.; Vacca, A.; Ghelli, S. *Anal. Bioanal. Chem.* **2003**, *376*, 1041−1052.

(21) (a) Thordarson, P. *Chem. Soc. Rev.* **2011**, *40*, 1305−1323. (b) Hunter, C. A.; Anderson, H. L. *Angew. Chem., Int. Ed.* **2009**, *48*, 7488−7499.

(22) (a) Wang, X.; Wicher, B.; Ferrand, Y.; Huc, I. *J. Am. Chem. Soc.* **2017**, *139*, 9350−9358. (b) Gan, Q.; Wang, X.; Kauffmann, B.; Rosu, F.; Ferrand, Y.; Huc, I. *Nat. Nanotechnol.* **2017**, *12*, 447−452.

(23) (a) Petersson, E. J.; Craig, C. J.; Daniels, D. S.; Qiu, J. X.; Schepartz, A. *J. Am. Chem. Soc.* **2007**, *129*, 5344−5345. (b) Collie, G. W.; Pulka-Ziach, K.; Lombardo, C. M.; Fremaux, J.; Rosu, F.; Decossas, M.; Mauran, L.; Lambert, O.; Gabelica, V.; Mackereth, C. D.; Guichard, G. *Nat. Chem.* **2015**, *7*, 871−878. (c) Sharma, G. V. M; Thodupunuri, P.; Sirisha, K.; Basha, S. J.; Gurava Reddy, P.; Sarma, A. V. S. *J. Org. Chem.* **2014**, *79*, 8614−8628. (d) De, S.; Chi, B.; Granier, T.; Qi, T.; Maurizot, V.; Huc, I. *Nat. Chem.* **2017**, *9*, DOI: 10.1038/nchem.2854.

DOI: 10.1021/jacs.7b07961
J. Am. Chem. Soc. 2017, 139, 14668−14675